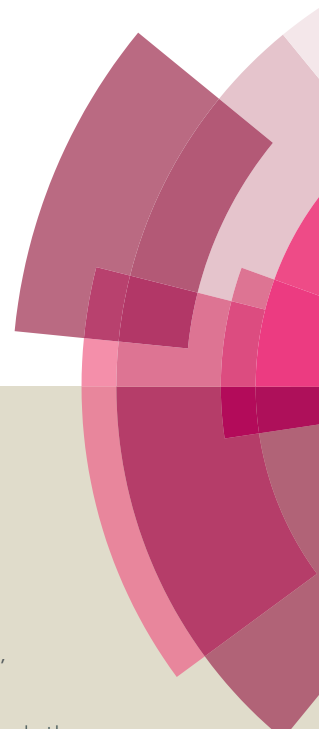


# Journal of Materials Chemistry B

Accepted Manuscript



This article can be cited before page numbers have been issued, to do this please use: L. Wang, Y. Yan, M. Wang, H. Yang, Z. Zhou, C. Peng and S. Yang, *J. Mater. Chem. B*, 2016, DOI: 10.1039/C5TB01910A.



This is an *Accepted Manuscript*, which has been through the Royal Society of Chemistry peer review process and has been accepted for publication.

*Accepted Manuscripts* are published online shortly after acceptance, before technical editing, formatting and proof reading. Using this free service, authors can make their results available to the community, in citable form, before we publish the edited article. We will replace this *Accepted Manuscript* with the edited and formatted *Advance Article* as soon as it is available.

You can find more information about *Accepted Manuscripts* in the [Information for Authors](#).

Please note that technical editing may introduce minor changes to the text and/or graphics, which may alter content. The journal's standard [Terms & Conditions](#) and the [Ethical guidelines](#) still apply. In no event shall the Royal Society of Chemistry be held responsible for any errors or omissions in this *Accepted Manuscript* or any consequences arising from the use of any information it contains.

## ARTICLE

# An Integrated Nanoplatfom for Theranostics *via* Multifunctional Core/Shell Ferrite Nanocubes

Cite this: DOI: 10.1039/x0xx00000x

Li Wang<sup>a</sup>, Yuping Yan<sup>a</sup>, Min Wang<sup>a</sup>, Hong Yang<sup>\*a</sup>, Zhiguo Zhou<sup>a</sup>, Chen Peng<sup>\*b</sup> and Shiping Yang<sup>\*a</sup>

Magnetic core/shell ferrite nanocubes (MNCs) were prepared by a two-step pyrolysis. MNCs not only exhibit an excellent magnetothermal effect, but also can be used as T<sub>2</sub> magnetic resonance (MR) imaging agents. To perform their good biocompatibility and targeting ability, MNCs were modified with poly(ethylene glycol) (PEG) and hyaluronic acid (HA). To further construct an integrated nanoplatfom for theranostics, doxorubicin (DOX) was loaded onto the surface of MNCs with the pH and heat-responsible chemical bond. Notably, MNCs revealed the great stability and magnetothermal effect. Moreover, they showed the negligible toxicity and synergistic therapy *in vitro*. Meanwhile, the MR imaging *in vivo* was further verified. The novel integrated nanoplatfom facilitates the excellent targeting MR imaging guided synergistic therapy of the magnetothermal and chemo-therapy. The multifunctional nanocubes will be capable of playing a vital role in future cancer therapy.

Received 00th Autumn 2015,  
Accepted 00th Autumn 2015

DOI: 10.1039/x0xx00000x

www.rsc.org/

## Introduction

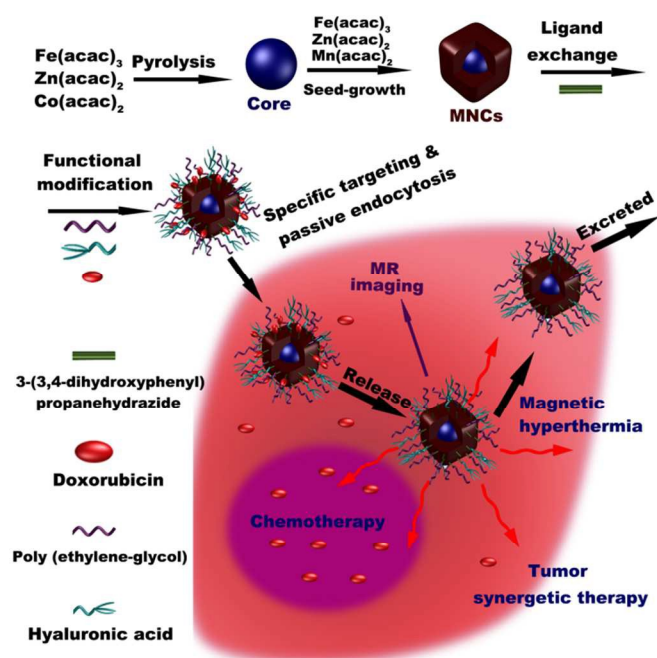
Cancer has been one of the main causes of death throughout the world for centuries. Though tremendous cancer therapies, such as surgery, chemotherapy, and radiotherapy, have been developed<sup>1,2</sup>, there are still the great risk for side effects and recurrence<sup>3</sup>. Therefore, it is necessary to search for the state-of-the-art therapeutic strategy to solve this problem. Recently, photothermal therapy (PTT)<sup>4-6</sup>, photodynamic therapy (PDT)<sup>7-9</sup>, magnetothermal therapy<sup>10-13</sup>, and chemotherapy<sup>14-17</sup>,<sup>18,19</sup> have been developed. Among these novel developed cancer therapies, magnetothermal therapy, which is powerful, non-invasive, harmless and has no problem of tissue penetration, has been the promising tumor treatment approach<sup>10,20,21</sup>. Magnetic nanoparticles (NPs) induce hyperthermia can generate efficient heat when they are subjected to an alternating magnetic field (AMF), which has been demonstrated in numerous cancer therapy<sup>10,12,13,21-23</sup>. Currently, they have been used in biomedicine fields mainly including Fe<sub>2</sub>O<sub>3</sub><sup>24,25</sup>, Fe<sub>3</sub>O<sub>4</sub><sup>26,27</sup> and MFe<sub>2</sub>O<sub>4</sub> (M = Mn, Zn, Co etc.)<sup>10,13</sup>. The heat generation under an AMF is resulted from Brownian and Néel relaxations of magnetic moments of NPs<sup>13</sup>. The chemical component, size, morphology, and crystal form of NPs have a crucial impart on the heat generation under an AMF. Furthermore, exchange-coupled magnetic NPs could result in the significant enhancement of the magnetothermal effect. Therefore, we prepared the exchange-coupled nanocubes (Zn<sub>0.4</sub>Co<sub>0.6</sub>)Fe<sub>2</sub>O<sub>4</sub> @ (Zn<sub>0.4</sub>Mn<sub>0.6</sub>)Fe<sub>2</sub>O<sub>4</sub> (denoted as MNCs) with the excellent magnetothermal effect<sup>13</sup>.

In order to improve the water solubility and targeting property of NPs, poly(ethylene glycol) (PEG) has been widely used for the modification because of its excellent performance *in vivo*<sup>28-34</sup>. It is

well known, hyaluronic acid (HA) is a targeting moiety to various cancer cells due to the specific interaction with overexpressed cluster determinant 44 (CD44)<sup>35-38</sup>. Considering the targeting property of HA to CD44 over-expressing cancer cells, HA modified MNCs were prepared for the targeted anti-cancer drug delivery<sup>38-40</sup>.

Various novel drug delivery strategies have been explored to improve the therapeutic effect<sup>41-44</sup>. Doxorubicin (DOX) is a classical anticancer drug and has been applied in patient treatment early. It has been reported that a drug delivery system by tethering DOX onto the surface of NPs *via* an acid-labile chemical bond can significantly inhibit the growth of cancer cells for the high efficiency of cellular uptake by endocytosis and subsequent acid responsive release in cancer cells<sup>45,46</sup>. In recent work, hyperthermic effect, magnetic hyperthermia/photothermal effect can increase the release kinetics of DOX<sup>47-49</sup>.

Inspired by the above mentioned reports, we developed an integrated nanoplatfom by modifying PEG, HA and DOX onto the surface of MNCs *via* the chemical reaction, which can significantly improve cancer therapy efficiency by taking advantage of the combined benefits from the functional units (Scheme. 1). Furthermore, the therapy effect of a novel integrated nanoplatfom *in vitro* has been demonstrated.



Scheme 1. The fabrication process of an integrated nanoplatform and the subsequent integrated tumor therapy

## Experimental

### Materials

Oleylamine, oleic acid, and 3-(3,4-dihydroxyphenyl)propanoic acid were purchased from Shanghai Sinopharm Chemical reagent Co., Ltd. 1,2-hexadecanediol and phenyl ether were purchased from TCI chemical Industry Co., Ltd. Hyaluronic acid (HA) and doxorubicin (DOX) were purchased from Alfa Aesar Chemical Co., Ltd.  $\text{Fe}(\text{acac})_3$ ,  $\text{Zn}(\text{acac})_2$ ,  $\text{Co}(\text{acac})_2$ ,  $\text{Mn}(\text{acac})_2$  were purchased from Sigma Adrich company. Water used in all experiments was purified using a Milli-Q Plus 185 water purification system (Millipore, Bedford, MA) with the resistivity higher than  $18 \text{ M}\Omega \cdot \text{cm}^{-1}$ .

**Synthesis of Zn- and Co-Doped iron oxide NPs [ $(\text{Zn}_{0.4}\text{Co}_{0.6})\text{Fe}_2\text{O}_4$  NPs].**  $\text{Fe}(\text{acac})_3$  (2 mmol),  $\text{Zn}(\text{acac})_2$  (0.4 mmol),  $\text{Co}(\text{acac})_2$  (0.6 mmol), 1,2-hexadecanediol (10 mmol), oleylamine (6 mmol), oleic acid (6 mmol), and phenyl ether (20 mL) were mixed and magnetically stirred under the flow of nitrogen. The reaction mixture was heated to  $200^\circ\text{C}$  for 2 h, then the temperature was increased to  $280^\circ\text{C}$  for another 1 h. The black-brown mixture was cooled to room temperature, then the black NPs were precipitated by ethanol, purified by the centrifugation and sonication, and dried overnight under the vacuum in sequence.

**Synthesis of Zn- and Mn-Doped iron oxide coated Zn- and Co-Doped Iron Oxide NPs [ $(\text{Zn}_{0.4}\text{Co}_{0.6})\text{Fe}_2\text{O}_4@(\text{Zn}_{0.4}\text{Mn}_{0.6})\text{Fe}_2\text{O}_4$  NPs, MNCs].** The synthesis of Zn- and Mn-doped iron oxide coated  $(\text{Zn}_{0.4}\text{Co}_{0.6})\text{Fe}_2\text{O}_4$  NPs was similar to that of  $(\text{Zn}_{0.4}\text{Co}_{0.6})\text{Fe}_2\text{O}_4$  NPs.  $\text{Fe}(\text{acac})_3$  (2 mmol),  $\text{Zn}(\text{acac})_2$  (0.4 mmol),  $\text{Mn}(\text{acac})_2$  (0.6 mmol), 1,2-hexadecanediol (10 mmol), oleylamine (2 mmol), oleic acid (2 mmol), the prepared NPs (84 mg) and phenyl ether (20 mL) were mixed and magnetically stirred under the flow of nitrogen. The reaction mixture was heated to  $200^\circ\text{C}$  for 1 h, then the temperature increased to  $280^\circ\text{C}$  for another 0.5 h. The other procedures were the same to the above step.

**Synthesis of poly(ethylene glycol) PEG modified MNCs (MNCs-PEG).** For the further functionalization of the obtained MNCs, the prepared 3-(3,4-dihydroxyphenyl)propanehydrazide ((DPPH) was synthesized according to the previous report<sup>51</sup>, which was verified by  $^1\text{H-NMR}$  (Fig. S1). DPPH conjugated methoxypoly(ethylene glycol) carboxyl acid (DPPH-PEG) was synthesized as follows. Methoxypoly(ethylene glycol) carboxyl acid (PEG-COOH, 20 mg), N-hydroxysuccinimide (NHS, 30 mg) and 3-(3-dimethylaminopropyl)-1-ethylcarbodiimide (EDC, 25 mg) were dissolved in pyridine (20 mL). After 2 h, DPPH (60 mg) was added to the above solution. The solution was reacted for 8 h, and 20 mg of the prepared MNCs was added, then the mixture was shaken for overnight. The obtained PEGylated MNCs (MNCs-PEG) were centrifuged and washed with ethanol and  $\text{H}_2\text{O}$ . The obtained MNCs-PEG were dispersed in water (10 mL) for further modification.

**Synthesis of HA modified MNCs-PEG (MNCs-PEG/HA)**<sup>52</sup>. HA (20 mg) was dissolved in 10 mL water, and heated to  $70^\circ\text{C}$ . Then EDC (50 mg) and NHS (100 mg) were added to the HA solution for the reaction of 2 h. The mixture was dropped into the above aqueous suspension of MNCs-PEG (20 mg, 10 mL) under ultrasound. After for 24 h in oscillators, the obtained HA modified MNCs-PEG (MNCs-PEG/HA) were subjected to multiple cycles of centrifugation/redispersion in water to remove the impurities.

**Synthesis of doxorubicin (DOX) modified MNCs-PEG/HA (MNCs-PEG/HA-DOX).** DOX (20 mg) was added to the aqueous suspension of 20 mL MNCs-PEG/HA (1 mg/mL). The mixed solution was reacted at  $50^\circ\text{C}$  in oscillators for 48 h. The prepared DOX modified MNCs-PEG/HA were centrifuged/ redispersed for 3 times and kept in water for further use.

**Magnetothermal experiments in the aqueous solution.** 2 mL of aqueous solution of MNCs-PEG/HA-DOX with different concentrations (50, 100, 200, and 500  $\mu\text{g}/\text{mL}$ , respectively) was placed into a 4 mL sample cell under an AMF (60.6 kA/m, 200 kHz) for 20 min. The temperature was recorded using a digital thermocouple device with an accuracy of  $\pm 0.1^\circ\text{C}$ . The specific loss power (SLP) was calculated using an equation (1). Where  $dT/dt$  is the initial slope of the heating curve,  $C$  is the volumetric specific heat capacity of the solution,  $V_s$  is the volume of the sample, and  $m$  is the mass of magnetic nanoparticles in the sample.

$$\text{SLP} = \frac{CV_s dT}{m dt} \quad (1)$$

**MR imaging in solution.** The longitudinal relaxation time ( $T_1$ ) and transverse relaxation time ( $T_2$ ) were measured (298 K) and  $T_2$ -weighted MR images were performed with a 0.5 T system (Shanghai Niumag Electronic Technology Co., Ltd, NM120-Analyst).  $T_1$ -weighted MR images were acquired using a conventional spin-echo sequence under the following parameters: TE = 12 ms, TR = 100 ms, 150 ms, 200 ms, 300 ms, 500 ms, 700 ms, 1000 ms, 1500 ms, 2500 ms,  $220 \times 320$  matrices,  $82 \times 120$  mm field of view, 140 Hz/Px of bandwidth, a slice thickness of 3 mm.  $T_2$ -weighted MR images using a fast spin-echo sequence was used to reduce acquisition time under the following parameters: TR = 1000 ms, TE = 13.8 ms, 27.6 ms, 41.4 ms, 55.2 ms, 69 ms, 82.8 ms,  $220 \times 320$  matrices,  $82 \times 120$  mm field of view, 220 Hz/Px of bandwidth, and a slice thickness of 3 mm. Longitudinal relaxation rate ( $r_1$ ) and transverse relaxation rate ( $r_2$ ) were calculated from the fitting of  $1/T_1$ ,  $1/T_2$  and metal ion concentration, respectively.

**Drug release in solution.** 3.0 mL of PBS buffer solution (pH 7.4 and 5.2, respectively) containing MNCs-PEG/HA-DOX (5 mg) was sealed in dialysis membranes (Mw cutoff = 3500). The dialysis bags were transferred to a cube containing PBS buffer solution (17 mL) of the same pH value at  $37^\circ\text{C}$  under the gentle shake ( $150 \text{ rpm min}^{-1}$ ). The amount of released DOX was recorded at the given time interval by a UV-vis spectrum

at 490 nm. Each experiment was repeated three times. The upper part (containing the sample in the dialysis cassette) was exposed to an AMF for 20 min before each measurement.

**Flow cytometry.** HeLa and U-87MG cells were seeded in 6-well culture plate with the density of  $2 \times 10^5$  cells per well in 2 mL of RPMI 1640 medium and incubated at 37 °C and 5 % CO<sub>2</sub>. After the incubation overnight, the medium was replaced with 2 mL fresh medium containing PBS buffer solution (control) or MNCs-PEG/HA-DOX. After 0, 5, 10, 15, 20, 30, 60, 120, and 240 min, respectively, the cells were washed with PBS, and then dealt with trypsin-EDTA solution (0.25%). Thereafter, the cells were separated by centrifugation and washed with PBS. The collected cells were re-suspended in 1 mL PBS and determined by flow cytometer (Cell Lab Quanta™ SC, Beckman Coulter). Flow Jo software 7.6.5 was used to analyze the data.

**Laser scanning confocal microscopy.** The cellular uptake process of MNCs-PEG/HA-DOX was also confirmed on laser scanning confocal microscopy (LSCM, Leica TCS SP5-II, Germany). After HeLa cells were incubated with MNCs-PEG/HA-DOX (100 µg/mL) for 0.5, 1, 2, and 4 h, respectively, excess MNCs-PEG/HA-DOX were removed by PBS. Then the cells were fixed with paraformaldehyde (2.5%) for 15 min, and stained with DAPI (100 ng/mL) for 15 min using a standard procedure. The cells on the coverslips were imaged using a 63 × oil-immersion objective lens. DOX and DAPI were excited by the 488 nm and 405 nm lasers, respectively.

**Magnetothermal therapy and chemotherapy *in vitro*.** HeLa cells were continuously cultured and seeded into 96-well cell culture plate at a density of  $5 \times 10^4$  cells/well in RPMI-1640 medium supplemented with 10% FBS and 1% penicillin-streptomycin at 37°C and 5% CO<sub>2</sub> for 24 h. After the incubation for 12 h, the medium was replaced by the different concentrations of MNCs-PEG/HA, MNCs-PEG/HA-DOX (0, 10, 20, 50, 100, and 200 µg/mL in RPMI-1640, respectively, DOX content in the samples is 0.625, 1.25, 2.5, 5, and 10 µg/mL, respectively), and DOX (0.625, 1.25, 2.5, 5, and 10 µg/mL) for 24 h at 37°C under 5% CO<sub>2</sub>. Meanwhile, the upper part incubated with MNCs-PEG/HA-DOX was exposed to an AMF for 20 min before a measurement. After removal of the medium, the purple formazan product was dissolved with DMSO for 15 min. Finally, the optical absorption of formazan at 490 nm was measured by an enzyme-linked immunosorbent assay reader (Multiskan MK3, USA.), and the background subtraction at 690 nm was applied.

**MR imaging *in vivo*.** The MR imaging *in vivo* was performed on HeLa tumor-bearing mice using a 3.0 T system (MAGNETOM VERIO, Siemens) before and after the tail injection of MNCs-PEG/HA-DOX of 0.5, 1, 2, 3, and 4 h, respectively. All animals were lawfully acquired and their retention and use were in every case in compliance with federal, state and local laws and regulations, and in accordance with the Institutional Animal Care and Use Committee of SLAC (IACUC) Guide for Care and Use of Laboratory Animals. T<sub>2</sub>-weighted MR images were acquired using a conventional spin-echo sequence with the following parameters: TR/TE = 7500/77, 256 × 256 matrices, 90 × 90 mm field of view, 140 Hz/Px of bandwidth, a slice thickness of 0.9 mm.

#### Characterization.

The morphology of materials was characterized using JEOLJEM-2010 transmission electron microscope. X-ray diffraction (XRD) was performed using a Rigaku DMAX 2000 diffractometer equipped with Cu/Kα radiation in the 2θ range from 20 to 80° ( $\lambda = 0.15405$  nm, 40 kV, 40 mA) at a scanning rate of 4°/min. The hydrodynamic

diameter and surface charge of NPs were obtained by dynamic light scattering (DLS) with a Malvern Zetasizer Nano ZS model ZEN3600. The sample absorbance was recorded on a Beckman Coulter DU 730 spectrophotometer. The hysteresis loops of NPs were measured on a Quantum Design SQUID MPM S XL-7.

## Results and discussion

### Synthesis and characterization of MNCs-PEG/HA-DOX

In this present work, (Zn<sub>0.4</sub>Co<sub>0.6</sub>)Fe<sub>2</sub>O<sub>4</sub> NPs were prepared according to the method reported<sup>50</sup>, which were monodispersed with an average diameter of  $7.6 \pm 1.4$  nm (Fig. 1a). The similar method was used to coat (Zn<sub>0.4</sub>Mn<sub>0.6</sub>)Fe<sub>2</sub>O<sub>4</sub> NPs to form core/shell NPs. TEM images of the core-shell structured (Zn<sub>0.4</sub>Co<sub>0.6</sub>)Fe<sub>2</sub>O<sub>4</sub>@(Zn<sub>0.4</sub>Mn<sub>0.6</sub>)Fe<sub>2</sub>O<sub>4</sub> nanocubes (MNCs) showed that the mean diameter was  $11.2 \pm 1.4$  nm (Fig. 1b). The increase of the diameter demonstrated that the successful construction of core/shell structure of MNCs. The crystallography of NPs was verified by powder X-ray diffraction (XRD) (Fig. S2). It is clear that all the diffraction peaks of the as-prepared (Zn<sub>0.4</sub>Co<sub>0.6</sub>)Fe<sub>2</sub>O<sub>4</sub> and MNCs can be indexed as an inverse spinel Fe<sub>3</sub>O<sub>4</sub> (JCPDS card No. 19-0629) phase. High resolution TEM image (Figure 1b inset) revealed the high crystalline nature of MNCs. The lattice spacing between two adjacent planes is 0.33 nm, which corresponds to the *d* spacing for the (220) lattice plane very well.

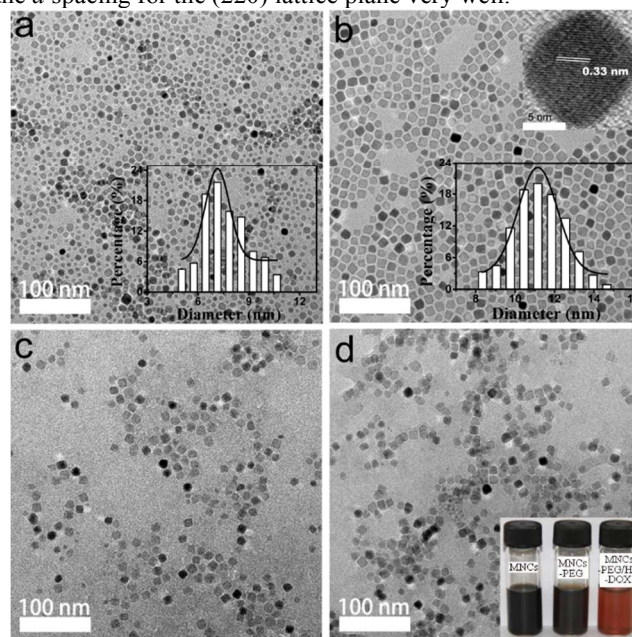


Fig. 1. TEM images of Zn<sub>0.4</sub>Co<sub>0.6</sub>Fe<sub>2</sub>O<sub>4</sub> NPs (a), MNCs (b), MNCs-PEG (c), and MNCs-PEG/HA-DOX (d). The bottom right inset in (a) and (b) is the size distribution of NPs. The top right inset in (b) is the HRTEM imaging of MNCs. The bottom right inset in (d) were the photographs of MNCs (in hexane), MNCs-PEG (in water), and MNCs-PEG/HA-DOX (in water), respectively. The scale bar is 100 nm and the scale bar of inset HRTEM is 5 nm.

It is well known that PEGylation is a successful strategy to endow NPs with the water solubility and biocompatibility. The amine moiety of 3-(3,4-dihydroxyphenyl)propanehydrazide (DPPH) on the surface of MNCs should be introduced for further graft of HA and DOX. In the first step, DPPH-PEG and

DPPH were coated on the surface of MNCs by the ligand exchange method. Then HA was reacted with a portion of the primary amine *via* an amide linkage to form MNCs-PEG/HA. MNCs-PEG/HA-DOX was obtained by conjugating DOX to MNCs-PEG/HA by a hydrazide linker.

To demonstrate the successful modification of PEG, HA and DOX, the thermogravimetric analysis (TGA) has been recorded firstly. The percentage contents of surfactants, PEG, HA and DOX were determined to be 8.4 %, 2.5%, 26.4 % and 3.9 %, respectively (Fig. S3). TEM images (Fig. 1c and 1d) showed that functionalized MNCs attained the similar morphology to those without PEG, HA and DOX modification, which were water dispersible (Fig. 1d inset). Zeta potential measurements showed that the surface potential increased from  $-30.4 \pm 1.4$  mV of MNCs-PEG to  $-45.7 \pm 0.9$  mV of MNCs-PEG/HA, which can be explained by the surface modification with negatively charged HA. MNCs-PEG/HA grafted with DOX on the surface of MNCs-PEG/HA gave rise to an increase of the surface potential, which resulted from the neutralization of the negative surface charge. It is clear that the characteristic band at 490 nm in the UV-vis spectroscopy (Fig. 2b) corresponded to the absorption of DOX, which verified the graft of DOX. The drug loading capacity was calculated to be  $\sim 50$   $\mu\text{g}/\text{mg}$ .

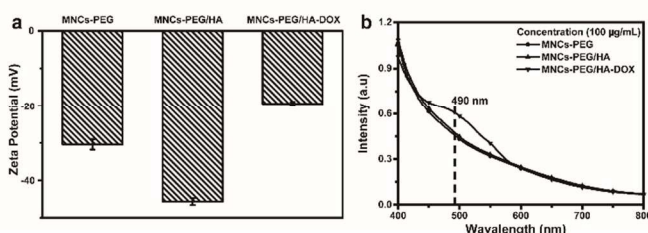


Fig. 2. The zeta potential (a), and UV-vis spectra (b) of MNCs-PEG, MNCs-PEG/HA, and MNCs-PEG/HA-DOX, respectively.

### Magnetic and relativity property

As the magnetic property of nanomaterials is crucial for their biomedical application, the hysteresis loops of MNCs, MNCs-PEG/HA and MNCs-PEG/HA-DOX were recorded firstly (Fig. S4). The saturation magnetization of MNCs was  $\sim 69$   $\text{emu g}^{-1}$  and decreased with the more ligand conjugated to MNCs. The hysteresis loop of MNCs-PEG/HA-DOX showed the remarkable superparamagnetic property. To validate the MR contrast ability, the longitudinal relaxation time ( $T_1$ ) and transverse relaxation time ( $T_2$ ) of MNCs-PEG/HA-DOX were examined in a 0.5 T MR system. The  $r_1$ ,  $r_2$  and  $T_2$ -weighted MR imaging were presented in Fig. 3a and 3b. The  $r_1$  and  $r_2$  value of MNCs-PEG/HA-DOX was 10.9 and 124.1  $\text{mM}^{-1}\text{s}^{-1}$ , respectively. It can be deduced that MNCs-PEG/HA-DOX should be a good candidate as  $T_2$  MR imaging agents. The  $T_2$ -weighted MR imaging of MNCs-PEG/HA-DOX (Fig. 3b) indicated the apparent  $T_2$ -weighted MR imaging effect.

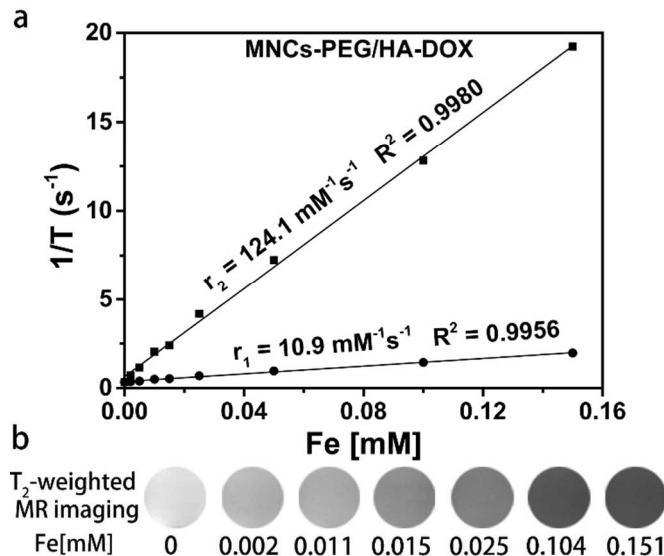


Fig. 3. The  $r_1$  and  $r_2$  values of MNCs-PEG/HA-DOX (a) and  $T_2$ -weighted MR imaging (b).

### Magneto-thermal and drug release property of MNCs-PEG/HA-DOX in solution

Magnetic hyperthermia therapy highly depends on the magneto-thermal effect of nanoparticles. Therefore, the SLP value of MNCs-PEG/HA-DOX was determined firstly. As seen from Fig. 4a, the temperature was elevated with the increase of the concentration of MNCs-PEG/HA-DOX. The SLP value of MNCs-PEG/HA-DOX was calculated to be  $\sim 1343.0$   $\text{W/g}$  by an equation (1). Under our alternative magnetic field condition, it is an excellent performance and laid the foundation for magnetic hyperthermia therapy. The acid-sensitive hydrazone linker can be cleaved effectively at low pH value. Therefore, the degradation of hydrazone bond of MNCs-PEG/HA-DOX will lead to the release of DOX.<sup>45,53</sup> To determine the drug release content, the absorbance at 490 nm was measured. As shown in Fig. 4b, the drug release profiles of DOX from MNCs-PEG/HA-DOX in PBS buffer solution (pH 7.4 and 5.3, respectively) at 37 °C were recorded, respectively. The result revealed that the release amount of DOX was up to  $\sim 26.8\%$  after 48 h in PBS at pH 7.4. However, when the pH of the solution was decreased to 5.3, 57.6% of DOX was released after 48 h in PBS at 5.3, which was attributed to the acceleration of cleavage of hydrazine bond at low pH value. Additionally, the heat of magneto-thermal effect also accelerated pH-responsive release of DOX from MNCs-PEG/HA-DOX. The cumulative content of DOX released from MNCs-PEG/HA-DOX under an AMF for 20 min increased to 38.8 and 87.4% at pH 7.4 and 5.3, respectively. It can be explained that an AMF induced the heat, which accelerated the cleavage of hydrazine bond and increased the efficiency of the drug release. Therefore, the magneto-thermal effect could be utilized as an external stimulus to effectively promote the drug release from MNCs-PEG/HA-DOX.

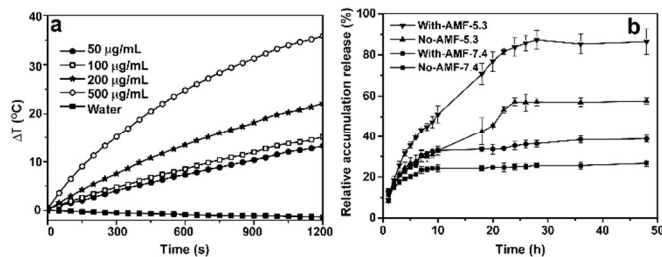


Fig. 4. (a) Heating curves of water and aqueous solution of MNCs-PEG/HA-DOX with different concentrations (50, 100, 200, and 500  $\mu\text{g/mL}$ , respectively) under an AMF (200 kHz, 60.6 kA/m). (b) The quantitative analysis of the released content of DOX from MNCs-PEG/HA-DOX with and without an AMF at pH 7.4 and 5.3, respectively.

### The property of MNCs-PEG/HA-DOX *in vitro*

To confirm the targeted ability of the MNCs-PEG/HA-DOX to cancer cells, both HeLa cells with CD44 receptor over-expression and U-87MG cells with CD44 receptor low-expression were incubated with MNCs-PEG/HA-DOX (100  $\mu\text{g/mL}$ ) for 0, 5, 10, 15, 20, 30, 60, 120, and 240 min, respectively. The amount of MNCs-PEG/HA-DOX uptaken by cancer cells was evaluated by the fluorescence intensity of DOX on the MNCs, which was determined by the flow cytometric analysis. By plotting the mean fluorescence intensity of HeLa cells and U-87MG cells as a function of time (Fig. 5a), we can see that HeLa cells showed remarkably higher fluorescence intensity than that of U-87MG cells, which indicated that the higher uptaken content of MNCs-PEG/HA-DOX to HeLa cells than that of U-87MG cells. To further confirm the receptor-mediated process of MNCs-PEG/HA-DOX in HeLa cells, the negative, temperature, and block control experiments were conducted (Fig. 5b). The incubation time of 1 h was selected for further investigation according to the relationship between the uptaken content of MNCs and incubation time. For the negative control experiment, U-87MG cells were chosen. After the incubation of 100  $\mu\text{g/mL}$  MNCs-PEG/HA-DOX, U-87MG cells of fluorescence signals decreased 54% relative to that of HeLa cells. As the incubation temperature decreased to 4°C, the fluorescence intensity of HeLa cells was also kept 55% compared with 37°C. For the block experiment, free HA was pre-incubated (30  $\mu\text{g/mL}$ ) with HeLa cells before the incubation with MNCs-PEG/HA-DOX, the fluorescence intensity of HeLa cells was decreased to 66% corresponding to the incubation with only MNCs-PEG/HA-DOX. These results indicated that the binding of MNCs-PEG/HA-DOX can be mediated by receptor-mediated endocytosis.

In order to figure out the DOX release process in HeLa cells, the fluorescence of HeLa cells was recorded for the different incubation of MNCs-PEG/HA-DOX by laser scanning confocal microscopy (CLSM). The CLSM images of the intracellular distribution of DOX (red color) and DAPI (blue color) were presented in Fig. S5. Apparently, the fluorescence of the cytoplasm became stronger with the increase of the incubation time. The overlay of red and blue color in nucleus illustrated that DOX had slowly transferred to nucleus. Subsequently, the DOX had an inhibiting effect on RNA and resulted in the cancer therapeutic effect. Additionally, the observed change of cellular morphology also indicated the therapeutic effect of DOX. The fact indicated that MNCs-PEG/HA-DOX firstly were taken up by cells *via* the specific targeted endocytosis, then DOX was released under the acid intracellular condition, transferred to nucleus, and played the therapeutic role.

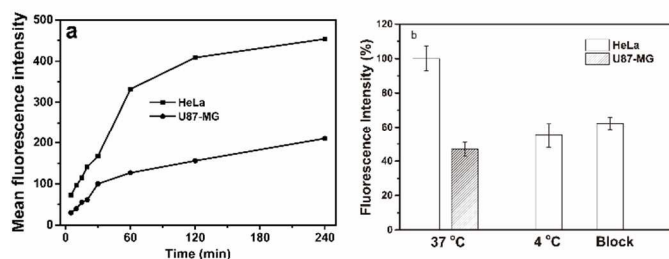


Fig. 5. (a) The mean fluorescence intensity of HeLa cells and U-87MG cells as a function of time. (b) The relative fluorescence intensity of HeLa cells and U-87MG cells were incubated with MNCs-PEG/HA-DOX (100  $\mu\text{g/mL}$ ) for 1 h at 37 °C and 4 °C, respectively. The block experiment: HA pre-incubated (30  $\mu\text{g/mL}$ ) U-87MG cells were then incubated with MNCs-PEG/HA-DOX (100  $\mu\text{g/mL}$ ) for 1 h at 37 °C.

### The synergetic therapy *in vitro*

According to the excellent magnetothermal effect and the high release efficiency of DOX of MNCs-PEG/HA-DOX in solution, the combined therapy for the enhanced effect for cancer cells was further verified. In our study, HeLa cells were incubated with free DOX, MNCs-PEG/HA and MNCs-PEG/HA-DOX with the same DOX concentration (0.625, 1.25, 2.5, 5, and 10  $\mu\text{g/mL}$ , respectively) (Fig. 6). When HeLa cells were only exposed under an AMF or incubated with MNCs-PEG/HA only, the killing effect on HeLa cells was negligible. The cell viability of HeLa cells incubated with free DOX or MNCs-PEG/HA, then exposed to an AMF showed the slight drop because of their chemotherapy effect of DOX and the magnetothermal effect of MNCs-PEG/HA, respectively. Remarkably, compared to the free DOX or MNCs-PEG/HA plus an AMF group, MNCs-PEG/HA-DOX incubated HeLa cells under an AMF showed the obviously low cell viability. Furthermore, with the increase of the incubation of MNCs-PEG/HA-DOX under an AMF, the cell viability decreased more and more. As we known, there are three possible factors accounting for the enhanced therapeutic effect. Firstly, the heat generated by MNCs-PEG/HA-DOX under an AMF improved the release of DOX. Secondly, the chemotherapy of DOX improved the sensitivity of cancer cells to heat. Lastly, the raised temperature also improved the sensitivity of cancer cells to DOX. Therefore, the combined therapy of chemotherapy and magnetic hyperthermia showed a synergetic therapy in HeLa cells.

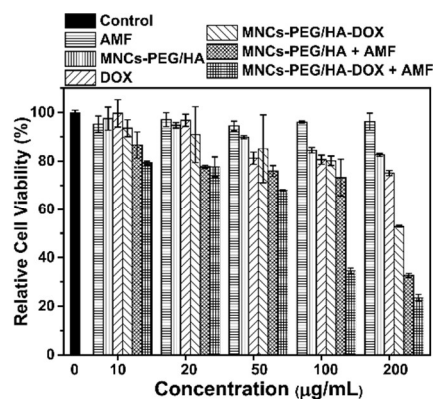


Fig. 6. The synergetic therapy to HeLa cells. Error bars were based on five parallel samples.

The MR imaging *in vivo* was carried out on HeLa tumor-bearing mice. The  $T_2$ -enhanced MR imaging was conducted on a 3 T MRI scanner before and after the tail vein injection of MNCs-PEG/HA-DOX (Fe: 0.10 mmol kg<sup>-1</sup>). The signal was darkened from 0.5 to 3 h gradually, and recovered at 4 h (Fig. 7a), which indicated the targeted diagnostic property. To our pity, the synergetic therapy *in vivo* hasn't performed with the limitation of our experiment condition.

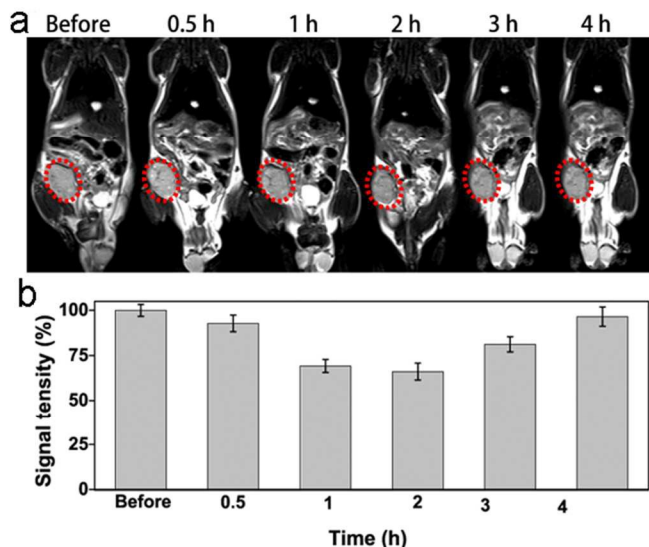


Fig. 7 (a) The MR imaging of mice before and after the tail vein injection of MNCs-PEG/HA-DOX.

### Conclusion

We constructed an integrated nanoplatform of MNCs-PEG/HA-DOX. The obtained MNCs-PEG/HA-DOX showed the large magnetothermal and  $T_2$ -weighted MR imaging effect. The good magnetothermal effect accelerated the pH release efficiency of DOX from MNCs-PEG/HA-DOX. The targeted MR imaging and effective synergetic therapy were further verified in HeLa cells. The MNCs-PEG/HA-DOX as a multifunctional nanoplatform could play an important role in other detection and therapeutic protocol. The further functionalization based on the MNCs and various use of the MNCs-PEG/HA-DOX could bring more attractive diagnosis and therapy strategies.

### Acknowledgements

This work was partially supported by National Natural Science Foundation of China (Nos.21271130, 21371122, and 81401458), Shanghai Science and Technology Development Fund (No. 13520502800), Shanghai Municipal Education Commission (Nos. 113ZZ110 and 14YZ073), and International Joint Laboratory on Resource Chemistry (IJLRC).

### Notes and references

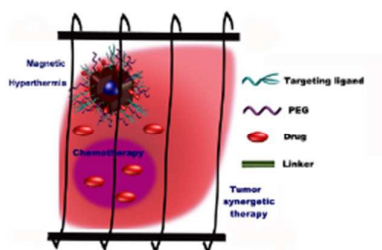
<sup>a</sup> The Key Laboratory of Resource Chemistry of Ministry of Education, Shanghai Municipal Education Committee Key Laboratory of Molecular Imaging Probes and Sensors, Shanghai Normal University, Shanghai 200234, China.

<sup>b</sup> Department of Radiology, Shanghai Tenth People's Hospital, Tongji University, Shanghai 200072, China

\*E-mail: yanghong@shnu.edu.cn, shipingy@shnu.edu.cn; Fax: 86-21-64322343.

1. D. S. Shewach and R. D. Kuchta, *Chem. Rev.*, 2009, **109**, 2859-2861.
2. L. Cheng, C. Wang, L. Feng, K. Yang and Z. Liu, *Chem. Rev.*, 2014, **114**, 10869-10939.
3. F. M. Kievit and M. Zhang, *Adv. Mater.*, 2011, **23**, H217-H247.
4. Q. Xiao, X. Zheng, W. Bu, W. Ge, S. Zhang, F. Chen, H. Xing, Q. Ren, W. Fan, K. Zhao, Y. Hua and J. Shi, *J. Am. Chem. Soc.*, 2013, **135**, 13041-13048.
5. J. He, X. Huang, Y.-C. Li, Y. Liu, T. Babu, M. A. Aronova, S. Wang, Z. Lu, X. Chen and Z. Nie, *J. Am. Chem. Soc.*, 2013, **135**, 7974-7984.
6. T. Liu, C. Wang, X. Gu, H. Gong, L. Cheng, X. Shi, L. Feng, B. Sun and Z. Liu, *Adv. Mater.*, 2014, **26**, 3433-3440.
7. S. Kim, T. Tachikawa, M. Fujitsuka and T. Majima, *J. Am. Chem. Soc.*, 2014, **136**, 11707-11715.
8. P. Kalluru, R. Vankayala, C.-S. Chiang and K.-C. Hwang, *Angew. Chem. Int. Ed.*, 2013, **52**, 12332-12336.
9. P. Huang, J. Lin, X. Wang, Z. Wang, C. Zhang, M. He, K. Wang, F. Chen, Z. Li, G. Shen, D. Cui and X. Chen, *Adv. Mater.*, 2012, **24**, 5104-5110.
10. J. Xie, Y. Zhang, C. Yan, L. Song, S. Wen, F. Zang, G. Chen, Q. Ding, C. Yan and N. Gu, *Biomaterials*, 2014, **35**, 9126-9136.
11. D. Yoo, H. Jeong, S.-H. Noh, J.-H. Lee and J. Cheon, *Angew. Chem.*, 2013, **125**, 13285-13289.
12. I. Marcos-Campos, L. Asin, T. E. Torres, C. Marquina, A. Tres, M. R. Ibarra and G. F. Goya, *Nanotechnology*, 2011, **22**, 205101.
13. J.-H. Lee, J.-t. Jang, J.-s. Choi, S. H. Moon, S.-h. Noh, J.-w. Kim, J.-G. Kim, I.-S. Kim, K. I. Park and J. Cheon, *Nat Nano*, 2011, **6**, 418-422.
14. L. Li, Y. Guan, H. Liu, N. Hao, T. Liu, X. Meng, C. Fu, Y. Li, Q. Qu, Y. Zhang, S. Ji, L. Chen, D. Chen and F. Tang, *ACS Nano*, 2011, **5**, 7462-7470.
15. A. M. Alkilany, L. B. Thompson, S. P. Boulos, P. N. Sisco and C. J. Murphy, *Adv. Drug Delivery Rev.*, 2012, **64**, 190-199.
16. H. Xu, Q. Yao, C. Cai, J. Gou, Y. Zhang, H. Zhong and X. Tang, *J. Control. Release*, 2015, **199**, 84-97.
17. M. Zhang and X. Shi, *J. Control. Release*, 2013, **172**, e55-e56.
18. Z. Liu, J. Shi, B. Jia, Z. Yu, Y. Liu, H. Zhao, F. Li, J. Tian, X. Chen, S. Liu and F. Wang, *Mol. Pharm.*, 2011, **8**, 591-599.
19. R. Kumar, J. Han, H.-J. Lim, W. X. Ren, J.-Y. Lim, J.-H. Kim and J. S. Kim, *J. Am. Chem. Soc.*, 2014, **136**, 17836-17843.
20. L. Asin, M. R. Ibarra, A. Tres and G. F. Goya, *Pharm. Res.*, 2012, **29**, 1319-1327.
21. Y. Qu, J. Li, J. Ren, J. Leng, C. Lin and D. Shi, *ACS Appl. Mater. Interfaces*, 2014, **6**, 16867-16879.
22. H. S. Huang and J. F. Hainfeld, *Int. J. Nanomed.*, 2013, **8**, 2521-2532.
23. S. Balivada, R. S. Rachakatla, H. Wang, T. N. Samarakoon, R. K. Dani, M. Pyle, F. O. Kroh, B. Walker, X. Leaym, O. Koper, M. Tamura, V. Chikan, S. H. Bossmann and D. L. Troyer, *BMC Cancer*, 2010, **10**, 119.

24. J.-P. Fortin, C. Wilhelm, J. Servais, C. Ménager, J.-C. Bacri and F. Gazeau, *J. Am. Chem. Soc.*, 2007, **129**, 2628-2635.
25. E. Alphandéry, S. Faure, O. Seksek, F. Guyot and I. Chebbi, *ACS Nano*, 2011, **5**, 6279-6296.
26. M. Gonzales-Weimuller, M. Zeisberger and K. M. Krishnan, *J. Magn. Magn. Mater.*, 2009, **321**, 1947-1950.
27. X. L. Liu, H. M. Fan, J. B. Yi, Y. Yang, E. S. G. Choo, J. M. Xue, D. D. Fan and J. Ding, *J. Mater. Chem.*, 2012, **22**, 8235-8244.
28. Z. Zhou, Y. Sun, J. Shen, J. Wei, C. Yu, B. Kong, W. Liu, H. Yang, S. Yang and W. Wang, *Biomaterials*, 2014, **35**, 7470-7478.
29. D. Ni, J. Zhang, W. Bu, H. Xing, F. Han, Q. Xiao, Z. Yao, F. Chen, Q. He, J. Liu, S. Zhang, W. Fan, L. Zhou, W. Peng and J. Shi, *ACS Nano*, 2014, **8**, 1231-1242.
30. S. Yoo, S. Hong, Y. Choi, J.-H. Park and Y. Nam, *ACS Nano*, 2014, **8**, 8040-8049.
31. A. S. Karakoti, S. Das, S. Thevuthasan and S. Seal, *Angew. Chem. Int. Ed.*, 2011, **50**, 1980-1994.
32. K. Knop, R. Hoogenboom, D. Fischer and U. S. Schubert, *Angew. Chem. Int. Ed.*, 2010, **49**, 6288-6308.
33. T. Sun, Y. S. Zhang, B. Pang, D. C. Hyun, M. Yang and Y. Xia, *Angew. Chem. Int. Ed.*, 2014, **53**, 12320-12364.
34. A. Berdichevski, Y. Shachaf, R. Wechsler and D. Seliktar, *Biomaterials*, 2015, **42**, 1-10.
35. K. Y. Choi, H. Chung, K. H. Min, H. Y. Yoon, K. Kim, J. H. Park, I. C. Kwon and S. Y. Jeong, *Biomaterials*, 2010, **31**, 106-114.
36. L. Li, Y. Qian, C. Jiang, Y. Lv, W. Liu, L. Zhong, K. Cai, S. Li and L. Yang, *Biomaterials*, 2012, **33**, 3428-3445.
37. H. Y. Yoon, H. Koo, K. Y. Choi, S. J. Lee, K. Kim, I. C. Kwon, J. F. Leary, K. Park, S. H. Yuk, J. H. Park and K. Choi, *Biomaterials*, 2012, **33**, 3980-3989.
38. Z. Wang, Z. Chen, Z. Liu, P. Shi, K. Dong, E. Ju, J. Ren and X. Qu, *Biomaterials*, 2014, **35**, 9678-9688.
39. H. Wu, H. Shi, Y. Wang, X. Jia, C. Tang, J. Zhang and S. Yang, *Carbon*, 2014, **69**, 379-389.
40. J.-H. Park, H.-J. Cho, H. Y. Yoon, I.-S. Yoon, S.-H. Ko, J.-S. Shim, J.-H. Cho, J. H. Park, K. Kim, I. C. Kwon and D.-D. Kim, *J. Control. Release*, 2014, **174**, 98-108.
41. J. Lu, W. Zhao, H. Liu, R. Marquez, Y. Huang, Y. Zhang, J. Li, W. Xie, R. Venkataramanan, L. Xu and S. Li, *J. Control. Release*, 2014, **196**, 272-286.
42. T. Ta, E. Bartolak-Suki, E.-J. Park, K. Karrobi, N. J. McDannold and T. M. Porter, *J. Control. Release*, 2014, **194**, 71-81.
43. S.M. Lee, H. J. Kim, S. Y. Kim, M.K. Kwon, S. Kim, A. Cho, M. Yun, J.S. Shin and K.H. Yoo, *Biomaterials*, 2014, **35**, 2272-2282.
44. R. Mo, T. Jiang and Z. Gu, *Angew. Chem. Int. Ed.*, 2014, **53**, 5815-5820.
45. F. Wang, Y.-C. Wang, S. Dou, M.-H. Xiong, T.-M. Sun and J. Wang, *ACS Nano*, 2011, **5**, 3679-3692.
46. S. Aryal, J. J. Graier, S. Pilla, D. A. Steeber and S. Gong, *J. Mater. Chem.*, 2009, **19**, 7879-7884.
47. H. Oliveira, E. Pérez-Andrés, J. Thevenot, O. Sandre, E. Berra and S. Lecommandoux, *J. Control. Release*, 2013, **169**, 165-170.
48. J. Shi, L. Wang, J. Zhang, R. Ma, J. Gao, Y. Liu, C. Zhang and Z. Zhang, *Biomaterials*, 2014, **35**, 5847-5861.
49. Z. Zhang, J. Wang and C. Chen, *Adv. Mater.*, 2013, **25**, 3869-3880.
50. S. Sun, H. Zeng, D. B. Robinson, S. Raoux, P. M. Rice, S. X. Wang and G. Li, *J. Am. Chem. Soc.*, 2004, **126**, 273-279.
51. Y. Gao, W. Jiang, S. Sun and J. Hou, in *State Intellectual Property Office of the People's Republic of China*, ed. L. Shandong green natural medicine research and development co., China, 2009.
52. J. Li, Y. Hu, J. Yang, P. Wei, W. Sun, M. Shen, G. Zhang and X. Shi, *Biomaterials*, 2015, **38**, 10-21.
53. Y. Bae, S. Fukushima, A. Harada and K. Kataoka, *Angew. Chem. Int. Ed.*, 2003, **42**, 4640-4643.



The novel integrated nanoplatform facilitates the excellent targeting MR imaging guided synergistic therapy of the magnetothermal and chemo-therapy based on magnetic core/shell ferrite nanocubes (MNCs).